Geosci. Model Dev. Discuss., 8, 4453–4486, 2015
www.geosci-model-dev-discuss.net/8/4453/2015/
doi:10.5194/gmdd-8-4453-2015
© Author(s) 2015. CC Attribution 3.0 License.

Geoscientific Model Development Discussions
Open Access

This discussion paper is/has been under review for the journal Geoscientific Model Development (GMD). Please refer to the corresponding final paper in GMD if available.

Assessment of valley cold pools and clouds in a very high resolution NWP model

J. K. Hughes[1], A. N. Ross[1], S. B. Vosper[2], A. P. Lock[2], and B. C. Jemmett-Smith[1]

[1]School of Earth and Environment, University of Leeds, Leeds, UK
[2]Met Office, Exeter, UK

Received: 20 April 2015 – Accepted: 26 May 2015 – Published: 16 June 2015

Correspondence to: J. K. Hughes (j.k.hughes@leeds.ac.uk)

Published by Copernicus Publications on behalf of the European Geosciences Union.

Abstract

The formation of cold air pools in valleys under stable conditions represents an important challenge for numerical weather prediction (NWP). The challenge is increased when the valleys which dominate cold pool formation are on scales unresolved by NWP models, which can lead to substantial local errors in temperature forecasts. In this study a two-month simulation is presented using a nested model configuration with a finest horizontal grid spacing of 100 m. The simulation is compared with observations from the recent COLPEX project and the model's ability to represent cold pool formation and the surface energy balance is assessed. The results reveal a bias in the model longwave radiation which results from the assumptions made about the sub-grid variability in humidity in the cloud parametrization scheme. The cloud scheme assumes relative humidity thresholds below 100 % to diagnose partial cloudiness, an approach common to schemes used in many other models. The biases in radiation, and resulting biases in screen temperature and cold pool properties are shown to be sensitive to the choice of critical relative humidity, suggesting that this is a key area which should be improved for very high resolution modelling.

1 Introduction

The stable boundary layer presents a difficult challenge for numerical simulation (Beare et al., 2006), it being associated with a rich variety of complex dynamical processes. The dominant eddy scales are smaller than those typical of convective boundary layers, turbulence is weak and intermittent (Van De Wiel et al., 2003) and the presence of internal gravity waves can have an important influence on drag and mixing. In complex terrain the flows are further complicated by drainage flows and the formation of valley cold pools which can result in minimum temperatures which are significantly lower than those above the surrounding higher terrain. Cold pools can lead to localized road icing and fog formation, presenting hazards to road users and frost damage to agriculture.

GMDD
8, 4453–4486, 2015

Previous studies of drainage flow and cold pools have tended to focus on large scale mountain valleys (e.g. Barr and Orgill, 1989; Lareau et al., 2013) or isolated bowls and sinkholes (e.g. Whiteman et al., 2008; Zängl, 2005). However, small scale valleys are also of practical importance and these are often unresolved even in modern NWP regional models which have grid spacing of a few kilometers.

These small scale valleys can nonetheless lead to significant temperature variations (Smith et al., 2010). The COLd air Pooling Experiment (COLPEX) was an investigation of the formation of cold air pools in such small-scale UK orography (Price et al., 2011). It combined high resolution modelling and observations for a field campaign in the Clun valley, Shropshire, UK from January 2009 to April 2010. The Clun valley is 1–2 km wide with a depth of 100–200 m and as such is not resolved in the Met Office regional UK forecast model, either at the 4 km horizontal resolution used operationally at the time, or at the current 1.5 km operational resolution. Cold air pools in this region can lead to local temperature differences of 5–10 K between hill top and valley bottom. Details of the observational campaign are described in Price et al. (2011). Sheridan et al. (2013) analysed the observed cold pool structure and related the frequency and strength of cold pools to previous idealised studies of cold pool formation (Vosper and Brown, 2008). Modelling work has used a nested version of the Met Office Unified Model (MetUM), with a horizontal grid spacing of 100 m. The basic model configuration and initial comparison with observations is given by Vosper et al. (2013a). The results show that the high horizontal and vertical resolution is required in order to sufficiently resolve the orography and obtain a good level of agreement between the simulated and observed temperature variations across the cold pools in clear-sky cases. Subsequently, Vosper et al. (2013b) focussed in detail on a single Intensive Observation Period (IOP) which took place on the night of 4 March 2010 (IOP 16). The latter study demonstrated the skill of the MetUM in reproducing the observed temperatures across the valley and provided a detailed analysis of the heat budget within the cold pool.

Previous modelling studies in COLPEX, and in other field campaigns, have used a case study approach, simulating short (2–3 day) events where cold air pools are

GMDD
8, 4453–4486, 2015

known to form. The current study takes a different approach with a two-month simulation at 100 m resolution in order to provide a longer term assessment of cold pool formation over the COLPEX region. This allows a more systematic and objective validation of the model representation of cold pools over a range of conditions. It also allows a quantification of the frequency, strength and drivers of cold air pools. Given the density of observations obtained in COLPEX this provides a good opportunity to validate the behaviour of the MetUM at high resolution over a range of conditions. The simulation also allows an investigation of the importance of spinning up the high-resolution model and can also be used to provide a more complete analysis of the synoptic scale influences on cold pool formation.

Two months is not sufficiently long to generate a true climatology, however the computational resources required to undertake a multi year simulation at this resolution are beyond what was available for this project. The current study provides a useful intermediate step towards this. Although not truly a climatology, we will refer to the two month simulation as a "climatology simulation" to contrast it from shorter, 1–2 day long case study simulations.

In the following sections the model configuration, the simulations and forcing data are described. Following this a discussion of the importance of model spin up is presented. From the climatological simulation an analysis of the temperature bias relative to observations is then given. Based on this analysis, an additional simulation is then presented and analysed. A comparison of simulated and observed cloud cover is then made with reference to unresolved humidity variability. The paper concludes with a more general discussion of the results.

GMDD
8, 4453–4486, 2015

2 Two month simulation over the COLPEX region

2.1 Model setup

The COLPEX simulations were conducted using the MetUM Model with a double-nested setup, with simulations running with horizontal grid spacings of 4, 1.5 km and 100 m (hereafter refered to as Δ4 km, Δ1.5 km and Δ100 m models). Vosper et al. (2013a) describe the modelling setup in detail so only a brief summary is given here. The innermost Δ100 m domain uses a non-uniform horizontal grid with the resolution decreasing from 100 m to 1.5 km at the boundaries (Tang et al., 2012). The domain covers a region of 80 km by 80 km, centred on the Clun Valley, Shropshire (UK) with a 30 km by 30 km inner domain of constant 100 m resolution. Figure 1 shows the innermost part of the domain including the Clun valley as represented in the 100 m simulations. Analysis data from the Met Office three-dimensional variational assimilation scheme (3D-VAR) is used to initialise the 4 km model and updates the Δ4 km state every three hours. The Δ4 km simulation then produces the lateral boundary conditions for Δ1.5 km which in turn produces lateral boundary conditions for the Δ100 m simulation. The nesting is one-way, with no feedback to lower resolutions. Δ1.5 km and Δ100 m simulations are "free-running", i.e. are not re-initialised during the simulation. This allows aspects such as soil moisture to develop spatial patterns consistent with the high resolution terrain data during the simulation rather than being constrained by relatively coarse analysis fields. The simulations presented here are all initialised at 12:00 UTC, allowing the model to spin up prior to the onset of stable conditions in the evening.

Other details of the model setup are broadly similar between resolutions, however there are a few key differences. Firstly, in the Δ100 m simulations the number of vertical levels is increased from 70 to 140. Secondly, different turbulence parametrisations are used at different resolutions. The Δ4 km model uses a 1-D boundary-layer scheme, while the Δ1.5 km uses a 2-D Smagorinsky turbulence parameterisation for horizontal mixing and a 1-D boundary layer scheme for vertical mixing, and the Δ100 m model

GMDD
8, 4453–4486, 2015

uses a 3-D Smagorinsky scheme (Lock et al., 2000). Finally, the vertical profile of critical relative humidity (RH_{crit}) necessary for cloud formation is increased, to take into account the reduction in grid box size (see Vosper et al., 2013a). The critical relative humidity threshold approach allows non-zero cloud cover to be diagnosed when grid box relative humidity is below saturation. This assumes that there is unresolved sub-grid scale variability in temperature and moisture which results in regions of cloud cover. This approach to sub-grid scale variability was first proposed by Sommeria and Deardorff (1977) and Mellor (1977). It was then developed into the form used here by Smith (1990). The critical relative humidity is a function of the standard deviation of sub-grid scale variability, such that when temperature and moisture variability are fully resolved the standard deviation of sub-grid scale variability is zero and RH_{crit} is 100 %. For the Δ1.5 km model the vertical profile of RH_{crit} is set to 91 % at the surface, reducing to 80 % at 845 m and constant at 80 % above. At Δ100 m this profile is set to 99 % in the lowest 500 m, decreasing linearly to 91 % at 3.4 km and constant (90 %) above this level. These profiles are shown in Fig. 2.

2.2 The simulations

The COLPEX observational field campaign ran between January 2009 and April 2010 (Price et al., 2011). A number of short simulations have been completed, corresponding to IOPs, some of which have been the focus of previous analysis (Sheridan et al., 2013; Vosper et al., 2013b). In addition to these, an extended simulation has been completed, for the period 17 August to 15 October 2009 (the climatology simulation). This period was chosen because it includes multiple IOP cases, two of which (9–10 September, IOPs 4 and 5) have already been investigated in detail (Price et al., 2011; Vosper et al., 2013a). The IOPs during this period include cases where the model reproduces the observations well (e.g. IOPs 4 and 5), and those where the model performs less well (16–17 September, IOP 6 and 7). In terms of investigating the mechanisms involved in cold pool formation it is appropriate to focus on IOPs where the model performs well,

GMDD
8, 4453–4486, 2015

however when the more general performance of the model is of interest it is important to consider a wider range of conditions over the whole two month period.

2.3 Continuity of 4 km analysis forcing data

The COLPEX simulations are reliant on archived operational 4 km UK analyses data from the Met Office 3D-VAR assimilation scheme. Unfortunately during 2009–2010 there are occasional instances of missing data from the archive. During the climatology simulation there were missing data during 5–7 September (18:00–14:00 UTC), 26–28 September (00:00–14:00 UTC) and on 4 October (09:00 to 14:00 UTC). It was beyond the resources of the current project to recreate the missing data. It was therefore necessary to understand and minimize the impact of the data gaps.

In order to retain as much of the system memory as possible, when the model is restarted after a period of missing forcing data the soil properties (soil moisture content and temperature) are initialised from the model state at the last equivalent time of day prior to the missing data. For example, when restarting the simulation at 12:00 UTC on 29 September the soil properties are initialised with those at 12:00 UTC on 25 September. Other, faster components of the simulation are simply downscaled, i.e. air temperature in the Δ100 m simulation at 12:00 UTC 29 September, is re-initialized with the Δ4 km air temperature. In tests this approach was shown to minimize the impact of the data gaps on the model evolution. To test this a period without data gaps was chosen. Temperature and moisture timeseries at the main observation sites of Spring Hill (hill-top) and Duffryn (bottom of the Clun valley) from the long Δ100 m simulation were compared with equivalent timeseries from simulations where the model was initialized using either the Δ100 m model state from 48 h previously, or by interpolating the Δ4 km solution to the 100 m grid. This analysis (not included here for brevity) led to the above approach.

GMDD
8, 4453–4486, 2015

2.4 Impact of spinning up the model state

One of the motivations for completing the climatology simulation is to quantify the importance of spinning up slower components of the model state (e.g. the soil properties) within the Δ100 m simulation. Completing multi-month simulations with this setup is currently very computationally expensive and the benefits of avoiding this are substantial. It is important to note, however, that soil properties in the shorter simulations are already spun up at the Δ4 km resolution. In downscaling to the Δ100 m simulation the soil temperatures are interpolated onto the Δ100 m grid and then adjusted relative to the height difference between orographic heights in the different resolutions using an assumed lapse rate of 6 K km^{-1}. This lapse rate was chosen from an analysis of soil temperature and orographic height variability in the Δ4 km output. Soil moisture is simply interpolated onto the Δ100 m grid.

Figure 3 shows the Δ100 m domain-averaged soil temperatures throughout the climatology run. The soil cools throughout August. At the start of September there is a significant warming trend (just prior to the first missing data period), before resuming the cooling trend. The lowest soil level shows an underlying trend which results from the extremely slow response time of this level. Figure 4 shows the domain-average soil moisture content throughout the climatology simulation on each soil level. Figures 3 and 4 show that there exists long term variability in the soil properties.

During the climatology simulation there are three pairs of IOPs: 9 and 10 September (IOP 4 and IOP 5), 16 and 17 September (IOP 6 and IOP 7), and 13 and 14 October (IOP 8 and IOP 9). Markers on Figs. 3 and 4 show domain-averaged soil temperature and moisture content from the IOP simulations. The initial domain-mean IOP soil temperatures are close to those in the climatology simulation. Figure 4 shows some difference in soil moisture between the IOP and climatology simulations, which is most pronounced after the moist event at the start of September. This suggests that there are differences in the hydrological cycle between the two resolutions since in the IOP

GMDD
8, 4453–4486, 2015

simulations the soil moisture content remains similar to the downscaled Δ4 km content throughout the simulation.

Figure 5 shows a comparison between the screen-level air temperature and specific humidity at the Duffryn site in the IOP and climatology simulations for the three IOP pairs. Figure 5 shows that in general the climatology simulation is not required in order to simulate the IOP cases, i.e. that the atmosphere adjusts relatively rapidly and that the temperature and humidity fields are not sensitive to the difference between soil properties in the Δ4 km and Δ100 m simulations. This supports the validity of earlier COLPEX work (e.g. Vosper et al., 2013b) and also suggests that the missing data periods in the climatology simulation do not undermine the analysis presented here.

3 Model temperature bias

Figure 6 shows the frequency distribution of biases in the daily minimum and maximum model screen-level (1.5 m) air temperature from the climatology simulation at the main observation sites, Duffryn (valley site) and Spring Hill (hill top site; see Fig. 1). All data are hourly averaged and differences are defined as model minus observed. Results from Δ100 m and Δ1.5 km resolutions are shown. Figure 6a shows that for Δ100 m the daily minimum temperature at Duffryn shows a stronger cold bias than at Spring Hill, i.e. at Duffryn there is a higher number of days where the minimum temperature is more than 3 K lower than observed. The mean bias at Duffryn is -1.6 ± 0.3 K and at Spring Hill it is -0.7 ± 0.2 K, where all errors stated are calculated as the standard error of the mean. For Δ1.5 km there is an apparent warm bias of 1.4 ± 0.3 K at Duffryn and 0.4 ± 0.2 K at Spring Hill. This warm bias at Duffryn is consistent with the fact that the valley is poorly resolved in the Δ1.5 km simulation.

Figure 6b shows that the simulated daily maximum temperatures have a general cold bias. For Δ100 m this cold bias is -0.6 ± 0.3 K at Duffryn and -0.9 ± 0.3 K at Spring Hill. In the Δ1.5 km simulation the mean biases are -1.1 ± 0.1 K at Duffryn and -0.1 ± 0.1 K at Spring Hill. If the Spring Hill temperatures are representative of temperatures

GMDD
8, 4453–4486, 2015

outside the valley this suggests that there is a widespread cold bias in the Δ100 m simulation that is not caused by bias in the lateral boundary conditions or present in the lower resolution simulations. The cold bias in Δ1.5 km at Duffryn is most likely due to unresolved sheltering effects, which would give rise to local daytime warming within the valley.

The difference between hill top (Spring Hill) and valley bottom (Duffryn) screen temperature gives a measure of the strength of cold air pooling in the Clun valley. Using this difference, Fig. 6c shows the frequency distribution of daily maximum cold pool strength in the Δ100 m and Δ1.5 km simulations and in the observations. For Δ100 m the model simulates more strong cold pool events than observed. The simulated mean Δ100 m cold pool strength is 2.4 ± 0.3 K, compared to an observed mean strength of 1.6 ± 0.3 K. Figure 6a and b shows this difference is due to the stronger cold bias at Duffryn. For Δ1.5 km the valley is not properly resolved and the apparent cold pool strength is typically close to zero; the mean is 0.4 ± 0.1 K.

3.1 Daily minimum temperature bias

Figure 7 shows the distribution of Δ100 m model daily minimum temperatures against observations at Duffryn. The strongest cold biases exist during relatively warm nights, whilst there is good agreement between model and observations during the coldest nights. The coldest nights are clear sky cases, suggesting that perhaps errors in the simulated cloud cover may contribute to the cold bias seen at higher temperatures. Previous COLPEX studies have focused on clear sky cases, since this is a prerequisite for strong cold pool formation (e.g. Vosper et al., 2013b) however Fig. 7 shows that a more general evaluation of the modelling setup should include other cases.

Whilst there were no in-situ direct measurements of cloud properties during this time at Duffryn or Spring Hill, downward longwave radiative flux is available and directly quantifies the impact of cloud on the nocturnal energy balance. Figure 8 shows the agreement between simulated (Δ100 m) and observed longwave radiative flux at Spring Hill. The relationship to the temperature bias is illustrated by colouring the mark-

GMDD
8, 4453–4486, 2015

ers based on the observed hourly temperature bias. Each panel shows all observations from the 2 month simulation in the daily 3 h window, with each circle showing a single hourly comparison. At both Spring Hill and Duffryn (not shown) sites there are a substantial number of days where downward longwave radiation is under predicted. This bias develops during the evening and persists through the morning. The size of the bias in longwave radiation is similar at both sites, with a mean daily bias of $-21.7 \pm 2.7\,\mathrm{W\,m^{-2}}$ at Duffryn and $-23.3 \pm 3.2\,\mathrm{W\,m^{-2}}$ at Spring Hill. The bias is smallest in the period 13:00–16:00 UTC at both sites when there is a mean model bias of $-6.0 \pm 2.9\,\mathrm{W\,m^{-2}}$. There is a systematic increase in this bias during the night and morning, increasing from $-24.4 \pm 2.9\,\mathrm{W\,m^{-2}}$ (19:00–22:00 UTC) to $-33.7 \pm 2.7\,\mathrm{W\,m^{-2}}$ (07:00–10:00 UTC). There is a substantial cold bias in all time periods in Fig. 8, however Fig. 8h in particular suggests that this cold bias is associated with the under predicted downwelling longwave radiation.

In the Δ1.5 km simulation the bias in downward longwave flux is smaller than seen in the Δ100 m model, the mean being $-10.1 \pm 2.4\,\mathrm{W\,m^{-2}}$, at Duffryn a reduction of 53 % compared to the Δ100 m model. At Spring Hill this value is $-7.2 \pm 2.4\,\mathrm{W\,m^{-2}}$ (a reduction of 69 %).

At this point we conclude that the daily minimum temperature in the Δ100 m simulation has a systematic cold bias, most likely caused by too little cloud cover in the Δ100 m simulation itself (in contrast to biases introduced via transport through the lateral boundaries). The fact that Duffryn exhibits a greater cold bias than Spring Hill is most likely due to the effects of resolved cold pool formation, which exacerbate the bias.

3.2 Daily maximum temperature

During the daytime shortwave radiation dominates the energy budget. Figure 9 shows the agreement between the simulated and observed downward shortwave radiative flux at Spring Hill, combined with the screen temperature bias in the Δ100 m model. As shown previously, the simulated mean daily maximum temperature exhibits a cold

GMDD
8, 4453–4486, 2015

bias. Figure 9 is consistent with this. Averaged between both stations, 89 % of data show a cold bias at the start of the day (07:00–10:00 UTC). This fraction decreases throughout the day, dropping to 71 % by 16:00–19:00 UTC. In contrast to this cold bias, downward shortwave radiation is over predicted on average, consistent with the reduction in frequency of cold bias data points. In the early morning and late evening (07:00–10:00 UTC and 16:00–19:00 UTC) the mean bias in shortwave radiation is $14.4 \pm 5.0\,\mathrm{W\,m^{-2}}$. Between 10:00 and 16:00 UTC the mean bias is $36.6\,\mathrm{W\,m^{-2}}$. During the afternoon, strong warm bias points (defined as those for which the model temperature is 1 K or more higher than observed) are associated with an over prediction of downwelling shortwave radiation, whilst strong cold bias points (bias ≤ -1 K) are typically associated with under predicted downwelling shortwave radiation, though in general cold bias points are evenly distributed between over and under predicted shortwave radiation. It seems likely, therefore that the cold bias in the daily minimum temperatures is the cause of the cold bias in daily maximum temperatures. It was hypothesised earlier that this is due to under prediction of cloud cover, and the observed over prediction of shortwave radiation also indicates too little cloud cover in the model at Δ100 m.

4 Impact of the RH_{crit} profile

The above analysis suggests that a cloud cover bias affects the general ability of the model to accurately simulate the observed temperatures. This is now verified by performing an additional simulation using a modified version of the Δ100 m model setup.

As described earlier, although there are only a minimal set of differences between the Δ100 m and Δ1.5 km configurations one difference is the prescribed vertical profile of the relative humidity threshold, RH_{crit}, above which cloud forms. The values are higher in the Δ100 m configuration, based on the assumption that there will be less sub-grid scale variability in humidity at higher resolution, since at sufficiently high resolution variability in temperature and humidity would be resolved. In order to test the

GMDD
8, 4453–4486, 2015

sensitivity of the simulation to cloud cover the prescribed vertical RH_{crit} profile in the Δ100 m simulation was replaced with a vertical profile equivalent to the Δ1.5 km profile, with values interpolated onto the Δ100 m vertical levels. The modified Δ100 m setup (hereafter refered to as Δ100 m_r) is then tested in an additional simulation.

Figure 8 showed that a bias in the Δ100 m downward longwave radiation exists throughout the night. This bias is pronounced during 15–25 September and is absent at coarser resolution (Δ1.5 km) over the same period, suggesting it is an internal feature of the Δ100 m simulation. This period also includes two IOPs (16–17 September; IOPs 6 and 7), allowing for a detailed comparison with observations, and so was chosen for a test of the Δ100 m_r configuration.

Figure 10 shows simulated mean vertical profiles of cloud fraction over the lowest 1 km for the Δ1.5 km, Δ100 m and Δ100 m_r simulations. As expected, comparing Fig. 10a and b shows a large decrease in cloud cover between the Δ1.5 km and original Δ100 m simulation. This decrease in cloud cover is largely due to the change in RH_{crit} profile, since reverting the RH_{crit} profile at Δ100 m to the Δ1.5 km profile results in cloud cover fractions similar to Δ1.5 km (Fig. 10c).

Figure 11a shows the vertical cloud profile averaged over the re-run period and averaged spatially over the inner domain of the Δ100 m (i.e. the central domain of the simulation with constant 100 m grid spacing). Figure 11b and c shows equivalent mean cloud profiles for day (07:00–19:00 UTC) and night (19:00–07:00 UTC) periods separately. In Fig. 11a the cloud cover over the lowest 100 m is similar in the Δ100 m and Δ100 m_r simulations but above this the Δ100 m_r cloud is close to that in the Δ1.5 km model. When the cloud profiles for day and night are separated, more substantial differences become apparent between Δ1.5 km and Δ100 m_r. During the day the Δ100 m_r cloud fraction is close to that of Δ1.5 km whereas the original Δ100 m cloud cover is consistently smaller. During the night Δ100 m_r produces more cloud over the lowest 500 m than Δ1.5 km and Δ100 m. Above 500 m the Δ100 m_r cloud is more similar to that of Δ1.5 km than Δ100 m. The diurnal variability in near surface air conditions is larger in Δ100 m than Δ1.5 km during 15–25 September. The domain and time aver-

GMDD
8, 4453–4486, 2015

aged Δ100 m near surface air has lower night temperatures, increased dew deposition and lower specific humidities than Δ1.5 km. The cooler temperatures dominate, leading to the observed increased cloud cover at Δ100 m irrespective of the RH_{crit} profile used (Fig. 11c).

Comparing the downward longwave radiation in the Δ100 m and Δ100 m_r simulations it is evident that the bias is reduced by reducing RH_{crit}, but not eliminated. The Δ100 m longwave radiation has a bias of $-59.4 \pm 17.3\,W\,m^{-2}$ averaged over 15–25 September and at both sites. For Δ100 m_r, this bias is $-43.1 \pm 18.1\,W\,m^{-2}$: a reduction of 27 %. Both Duffryn and Spring Hill show similar biases. For the same period, the Δ1.5 km downward longwave radiation has a similar bias to the Δ100 m_r output, with a mean bias of $-44.2 \pm 18.1\,W\,m^{-2}$, suggesting that there is a residual bias, perhaps connected with errors in the 4 km driving model over this period. Note that 15–25 September was chosen as a period during which there is substantial bias in the simulation. The model longwave bias of Δ1.5 km averaged over the whole of the climatology period is $-8.7\,W\,m^{-2}$ (see Sect. 3.1).

During the re-run period downward shortwave radiation in the Δ100 m simulation is over predicted by $59.1 \pm 17.4\,W\,m^{-2}$ (considering all data between 0700 and 1859 h at both sites). In the Δ100 m_r simulation this bias is reduced to $11.2 \pm 15.8\,W\,m^{-2}$, again suggesting improved cloud cover.

In general, screen-level temperatures agree more closely with observed temperatures in the Δ100 m_r simulation than the Δ100 m simulation. Over the re-run period the mean temperature bias is reduced from −1.1 to −0.3 K at Duffryn and from −0.9 to −0.5 K at Spring Hill. Daily maximum temperatures are within 0.5 K of observed maxima during this period (for both RH_{crit} profiles) and do not systematically improve with the updated profile (the bias at Duffryn changes from 0.3 to 0.1 K whilst at Spring Hill the bias changes from −0.02 to −0.3 K). Daily minimum temperatures do systematically improve, with bias at Duffryn changing from −2.3 to −0.2 K and the bias at Spring Hill changing from −1.5 to −0.7 K.

GMDD
8, 4453–4486, 2015

The impact of these changes on simulated cold pool strength is shown in Fig. 12, which illustrates how changing the RH_{crit} profile reduces the number of nights in which cold pools develop, more closely matching the observed cold pool variability over this period.

Since the re-run period was chosen to include two IOP cases (16–17 September; IOP 6 and 7) it is also possible to compare simulated cloud profiles against radiosonde profile data. Figure 13 compares Δ1.5 km model cloud cover profiles with radiosonde profiles at Spring Hill. Radiosondes were released hourly from Spring Hill and Duffryn during the evenings of 16 and 17 September. Both nights show high relative humidity at heights between 500 m and 1 km, in particular during the night of the 17 September when the air is near saturated between 700 m and 1 km throughout the night. This is in reasonable agreement with cloud cover in the Δ1.5 km simulation and Figs. 10 and 13 demonstrate that not only does the updated RH_{crit} profile result in cloud cover at 100 m resolution which is similar to that in the Δ1.5 km simulation, it also produces cloud cover which is in better agreement with observations.

As discussed earlier, the model critical relative humidity threshold is designed to account for unresolved variability in the humidity and temperature fields. It is therefore reasonable to expect that as resolution increases, the fraction of resolved variability increases and the appropriate RH_{crit} increases towards 100 % (variability fully resolved). In order to quantify this, variability was calculated as the spatial standard deviation of relative humidity at each model height at each hour during the 10 day re-run period. These profiles were then time-averaged. Figure 14 shows vertical profiles of relative humidity standard deviation. Also included in Fig. 14 are profiles for Δ100 m model output which prior to analysis have been horizontally averaged to 1.5 km resolution. Away from the land surface RH standard deviation is greatest in Δ100 m as expected, and similar in both Δ1.5 km and the reduced resolution Δ100 m data. However, Fig. 14 also shows that close to the land surface differences in the surface energy balance between the model resolutions dominate and result in higher RH standard deviation in Δ1.5 km than the higher resolution simulation. This is particularly pronounced during nights. As

GMDD
8, 4453–4486, 2015

was noted earlier there are differences in the domain-averaged near surface conditions between model versions and Δ100 m is cooler and drier at night than Δ1.5 km, resulting in lower RH variability in Δ100 m than Δ1.5 km.

5 Conclusions

A high resolution, two month simulation of the flow in Clun valley has been produced, allowing an analysis of the base model climatology as well as producing a robust assessment of the ability of the MetUM to capture the variability and strength of cold pool formation. By comparing a two month simulation to a series of shorter, IOP, simulations it was demonstrated that short simulations provide accurate results without the requirement to spin up slowly evolving components of the model at the highest resolution. Within the context of COLPEX this is an important result as it validates the approach taken in previous studies which have only made use of shorter simulations. It is a useful result in general since it supports the scientific validity of future high resolution simulations, without the requirement for computationally expensive extended simulations.

In addition to testing the importance of extended spin up times, the longer simulation also allowed an assessment of the model climatology. Daily minimum temperatures were shown to have a cold bias in the highest resolution simulations relative to observations. This bias was then demonstrated to be due to choices made within the cloud scheme about sub-grid humidity variability. Compared to the 1.5 km resolution simulation (Δ1.5 km), the original 100 m simulation (Δ100 m) predicted less cloud cover. Δ1.5 km also compared better with radiosonde observations made during an IOP.

As a sensitivity test a period in the climatology simulation was re-run, during which the bias in downward longwave radiation at Δ100 m was most pronounced. For this simulation (Δ100 m_r) the vertical profile of RH_{crit} at 100 m resolution used the 1.5 km model profile, i.e. no change in sub-grid scale variability between resolutions was assumed. This reduced the differences in model cloud cover between the resolutions.

GMDD
8, 4453–4486, 2015

The bias in the downward longwave radiative flux in the Δ100 m_r simulations was also reduced relative to the observations and this resulted in a reduction in the cold bias of daily minimum temperature and an improved simulation of cold pool variability. This demonstrates the importance of considerations of sub-grid-scale variability for accurate simulation at very high resolution. Two clear sky case IOPs, 9 September (IOP 4) and 4 March (IOP 16) have been analysed in previous studies (Vosper et al., 2013a, b) and it is important to note that when simulations of these IOPs were re-run with the Δ100 m_r setup there was negligible impact on the results, since both model and observations indicate clear sky conditions. The original Δ100 m model output accurately predicts the observed temperature in these IOPs, consistent with the analysis presented here which shows that the model is well formulated for clear-sky nights. Numerical weather prediction (NWP) models are increasingly being run at resolutions more traditionally associated with large eddy simulations. Moving into this regime presents a number of challenges since at horizontal grid spacing of 100–1000 m models will only partially resolve eddies (Wyngaard, 2004; Hong and Dudhia, 2011), a domain refered to as the grey zone (Honnert et al., 2011). In the convective boundary layer, the dominant eddy length scales are typically around 1 km in size, approaching the depth of the boundary layer and therefore most likely resolved by the current modelling setup (Wyngaard, 1990). However stable boundary layer eddies have smaller dominant eddy scales (Wyngaard, 1990) and will be poorly resolved at 100 m resolution. Shin and Hong (2013) for example, completed a range of simulations varying the model resolution, demonstrating this sensitivity to the atmospheric stability. Investigating the resolution sensitivity of large eddy simulations of the stable boundary layer, Beare and Macvean (2004) showed a convergence of model behaviour only as horizontal resolution approached 2 m.

Interestingly, in contrast to the results of our study Boutle et al. (2014) investigated stratocumulus simulations in the grey zone and found relatively little sensitivity to the choice of RH_{crit}. This discrepency suggests the application of a more sophisticated approach to representing unresolved variability in saturation, in which the assumed

GMDD
8, 4453–4486, 2015

sub-grid variability is not static but instead varies according to properties of the flow. Watanabe et al. (2009) for example developed such a scheme with a dynamic representation of the unresolved PDFs. Such an approach has the potential to circumvent the need to specify RH_{crit} values and may be more appropriate.

Acknowledgements. We would like to thank everyone involved in the COLPEX field campaign. John Hughes' contribution was funded by the UK Natural Environment Research Council and UK Met Office through the Joint Weather and Climate Research Programme under grant NE/I007679/1. We acknowledge use of the MONSooN system, a collaborative facility supplied under the Joint Weather and Climate Research Programme, a strategic partnership between the Met Office and the Natural Environment Research Council.

References

Barr, S. and Orgill, M. M.: Influence of external meterology on nocturnal valley drainage winds, J. Appl. Meteorol., 28, 497–517, doi:10.1175/1520-0450(1989)028<0497:IOEMON>2.0.CO;2, 1989. 4455

Beare, R. and Macvean, M.: Resolution sensitivity and scaling of large-edy simulations of the stable boundary layer, Bound.-Lay. Meteorol., 112, 257–281, doi:10.1023/B:BOUN.0000027910.57913.4d, 2004. 4469

Beare, R. J., Macvean, M. K., Holtslag, A. A. M., Cuxart, J., Esau, I., Golaz, J. C., Jimenez, M. A., Khairoutdinov, M., Kosovic, B., Lewellen, D., Lund, T. S., Lundquist, J. K., Mccabe, A., Moene, A. F., Noh, Y., Raasch, S., and Sullivan, P.: An intercomparison of large-eddy simulations of the stable boundary layer, Bound.-Lay. Meteorol., 118, 247–272, doi:10.1007/s10546-004-2820-6, 2006. 4454

Boutle, I., Eyre, J., and Lock, A. P.: Seamless stratocumulus simulation across the turbulent gray zone, Mon. Weather Rev., 142, 1655–1668, doi:10.1175/MWR-D-13-00229.1, 2014. 4469

Hong, S. and Dudhia, J.: Next-generation numerical weather prediction: bridging parameterization, explicit clouds, and large eddies, B. Am. Meteorol. Soc., 93, ES6–ES9, doi:10.1175/2011BAMS3224.1, 2011. 4469

GMDD
8, 4453–4486, 2015

Honnert, R., Masson, V., and Couvreux, F.: A diagnostic for evaluating the representation of turbulence in atmospheric models at the kilometric scale, J. Atmos. Sci., 68, 3112–3131, doi:10.1175/JAS-D-11-061.1, 2011. 4469

Lareau, N. P., Crosma, E., Whiteman, C. D., Horel, J. D., Hoch, S. W., Brown, W. O. J., and Horst, T. W.: The persistent cold-air pool study, B. Am. Meteorol. Soc., 94, 51–63, doi:10.1175/BAMS-D-11-00255.1, 2013. 4455

Lock, A., Brown, A., Bush, M., Martin, G., and Smith, R.: A new boundary layer mixing scheme. Part I: Scheme description and single-column model tests, Mon. Weather Rev., 128, 3187–3199, doi:10.1175/1520-0493(2000)128<3187:ANBLMS>2.0.CO;2, 2000. 4458

Mellor, G.: Gaussian cloud model relations, J. Atmos. Sci., 34, 356–358, doi:10.1175/1520-0469(1977)034<0356:TGCMR>2.0.CO;2, 1977. 4458

Price, J. D., Vosper, S., Brown, A., Ross, A., Clark, P., Davies, F., Horlacher, V., Claxton, B., McGregor, J. R., Hoare, J. S., Jemmett-Smith, B., and Sheridan, P.: COLPEX field and numerical studies over a region of small hills, B. Am. Meteorol. Soc., 92, 1636–1650, doi:10.1175/2011BAMS3032.1, 2011. 4455, 4458, 4473

Sheridan, P. F., Vosper, S. B., and Brown, A. R.: Characteristics of cold pools observed in narrow valleys and dependence on external conditions, Q. J. Roy. Meteor. Soc., 140, 715–728, doi:10.1002/qj.2159, 2013. 4455, 4458

Shin, H. and Hong, S.-Y.: Analysis of resolved and parameterized vertical transports in convective boundary layers at gray-zone resolutions, J. Atmos. Sci., 70, 3248–3261, doi:10.1175/JAS-D-12-0290.1, 2013. 4469

Smith, R. N. B.: A scheme for predicting layer clouds and their water content in a general circulation model, Q. J. Roy. Meteor. Soc., 116, 435–460, doi:10.1002/qj.49711649210, 1990. 4458

Smith, S. A., Brown, A. R., Vosper, S. B., Murkin, P. A., and Veal, A. T.: Observations and simulations of cold air pooling in valleys, Bound.-Lay. Meteorol., 134, 85–108, doi:10.1007/s10546-009-9436-9, 2010. 4455

Sommeria, G. and Deardorff, J. W.: Subgrid-scale condensation in models of nonprecipitating cloud, J. Atmos. Sci., 34, 344–355, doi:10.1175/1520-0469(1977)034<0344:SSCIMO>2.0.CO;2, 1977. 4458

Tang, T., Lean, H. W., and Bornemann, J.: The benefits of the Met Office variable resolution NWP model for forecasting convection, Meteorol. Appl., 20, 417–426, doi:10.1002/met.1300, 2012. 4457

GMDD
8, 4453–4486, 2015

Van De Wiel, B. J. H., Moene, A. F., Hartogensis, O. K., De Bruim, H. A. R., and Holtslag, A. A. M.: Intermittent turbulence in the stable boundary layer over land. Part III: A classification for observations during CASES-99, J. Atmos. Sci., 60, 2509–2522, doi:10.1175/1520-0469(2003)060<2509:ITITSB>2.0.CO;2, 2003. 4454

Vosper, S. B. and Brown, A. R.: Numerical simulations of sheltering in valleys: the formation of night-time cold-air pools, Bound.-Lay. Meteorol., 127, 429–448, doi:10.1007/s10546-008-9272-3, 2008. 4455

Vosper, S. B., Carter, E., Lean, H., Lock, A., Clark, P., and Webster, S.: High resolution modelling of valley cold pools, Atmos. Sci. Lett., 14, 193–199, doi:10.1002/asl2.439, 2013a. 4455, 4457, 4458, 4469, 4486

Vosper, S. B., Hughes, J. K., Lock, A. P., Sheridan, P. F., Ross, A. N., Jemmett-Smith, B., and Brown, A. R.: Cold-pool formation in a narrow valley, Q. J. Roy. Meteor. Soc., 140, 699–714, doi:10.1002/qj.2160, 2013b. 4455, 4458, 4461, 4462, 4469

Watanabe, M., Emori, S., Satoh, M., and Miura, H.: A PDF-based hybrid prognostic cloud scheme for general circulation models, Clim. Dynam., 33, 795–816, doi:10.1007/s00382-008-0489-0, 2009. 4470

Whiteman, C. D., Muschinski, A., Zhong, S., Fritts, D., Hoch, S. W., Hahnenberger, M., Yao, W., Hohreiter, V., Behn, M., Cheon, Y., Clements, C. B., Horst, T. W., Brown, W. O. J., and Oncley, S. P.: Metcrax 2006 Meteorological Experiments in Arizona's Meteor Crater, B. Am. Meteorol. Soc., 89, 1665–1680, doi:10.1175/2008BAMS2574.1, 2008. 4455

Wyngaard, J.: Scalar fluxes in the planetary boundary layer – theory, modeling, and measurement, Bound.-Lay. Meteorol., 50, 49–75, doi:10.1007/BF00120518, 1990. 4469

Wyngaard, J.: Toward numerical modeling in the terra incognita, J. Atmos. Sci., 61, 1816–1826, doi:10.1175/1520-0469(2004)061<1816:TNMITT>2.0.CO;2, 2004. 4469

Zängl, G.: Formation of extreme cold-air pools in elevated sinkholes: an idealized numerical process study, Mon. Weather Rev., 133, 925–941, doi:10.1175/MWR2895.1, 2005. 4455

GMDD
8, 4453–4486, 2015

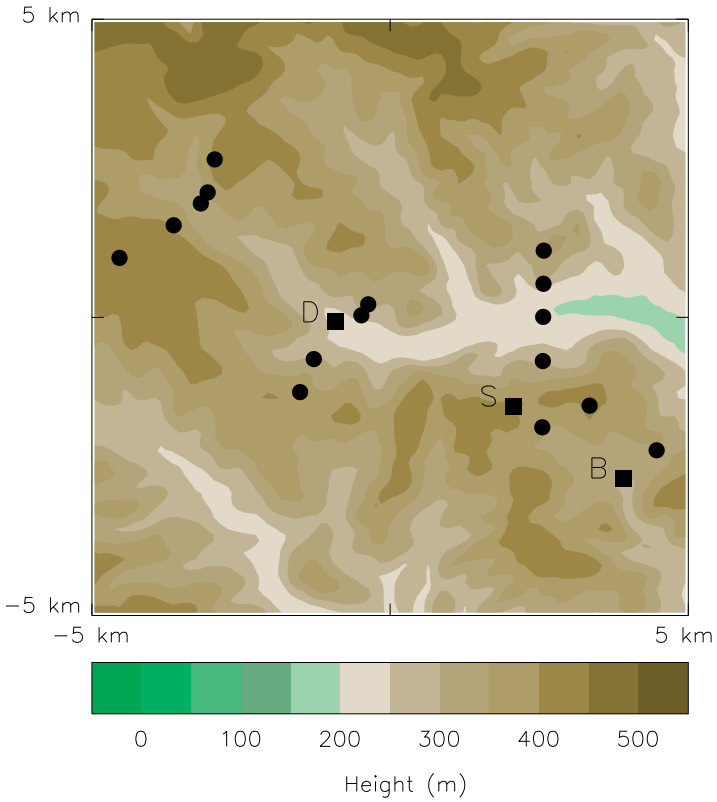

Figure 1. Orography of the Clun valley and surrounding region, as represented in the COLPEX Δ100 m simulations. The main observational tower sites are marked as squares and labelled. Hobo stations are marked with circles (see Price et al., 2011). The main sites are Duffryn (D; main valley, height 243 m), Springhill (S; local ridgetop, height 404 m) and Burfield (B; secondary valley, height 303 m). It should be noted that the full domain of the Δ100 m simulation is more extensive than is shown here.

GMDD
8, 4453–4486, 2015

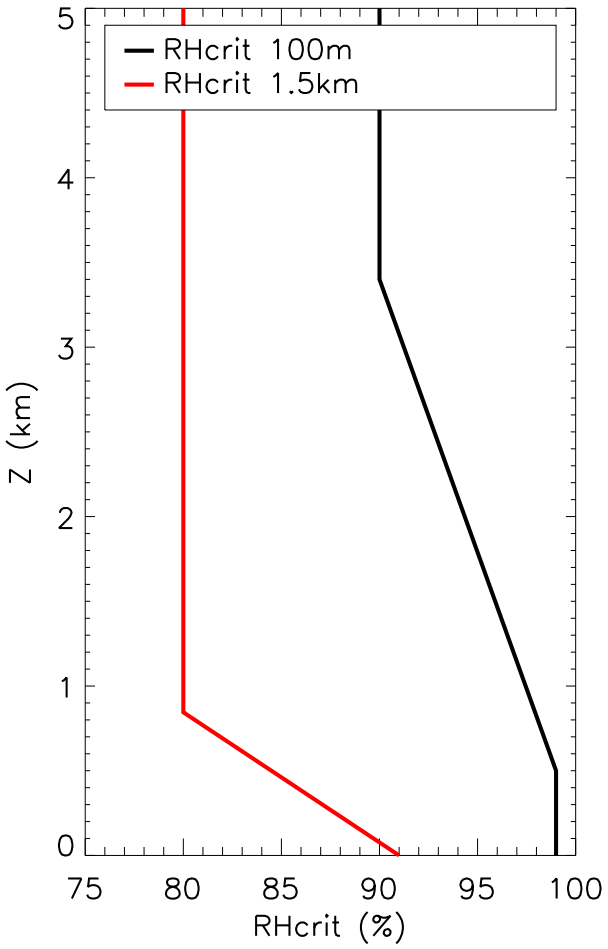

Figure 2. Vertical profiles of RH_{crit} used in the different nested models. The Δ100 m and Δ1.5 km profiles are shown in black and red, respectively.

GMDD
8, 4453–4486, 2015

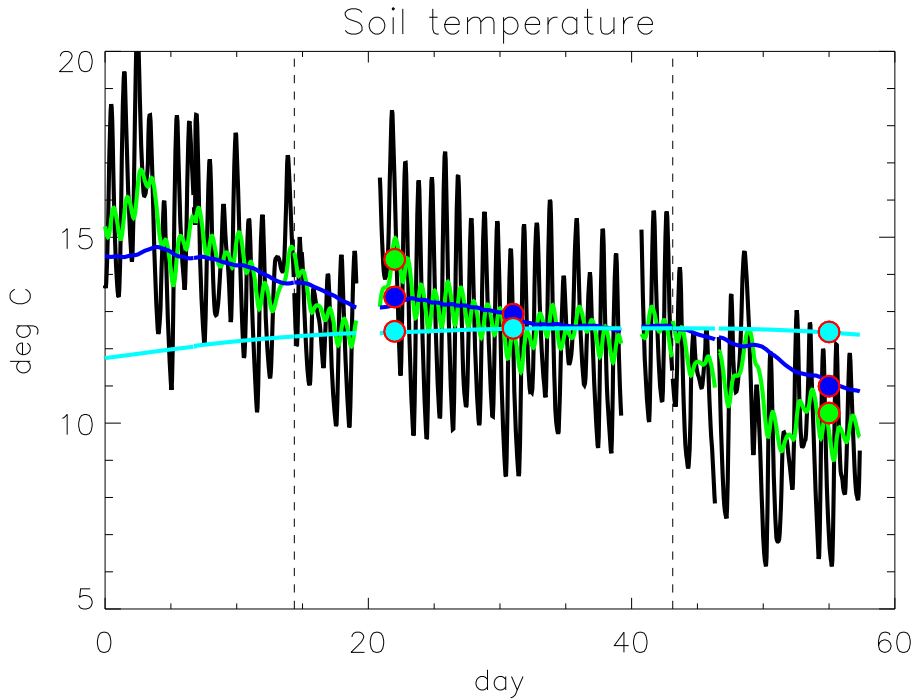

Figure 3. Evolution of the domain mean soil temperature. Day number corresponds to the day since the start of the climatology simulation. The soil levels shown are 0.05 m (black), 0.225 m (green), 0.675 m (dark blue) and 2 m (light blue). Shaded circles show the values from corresponding IOP simulations. Vertical dashed lines mark 1 September and 1 October.

GMDD
8, 4453–4486, 2015

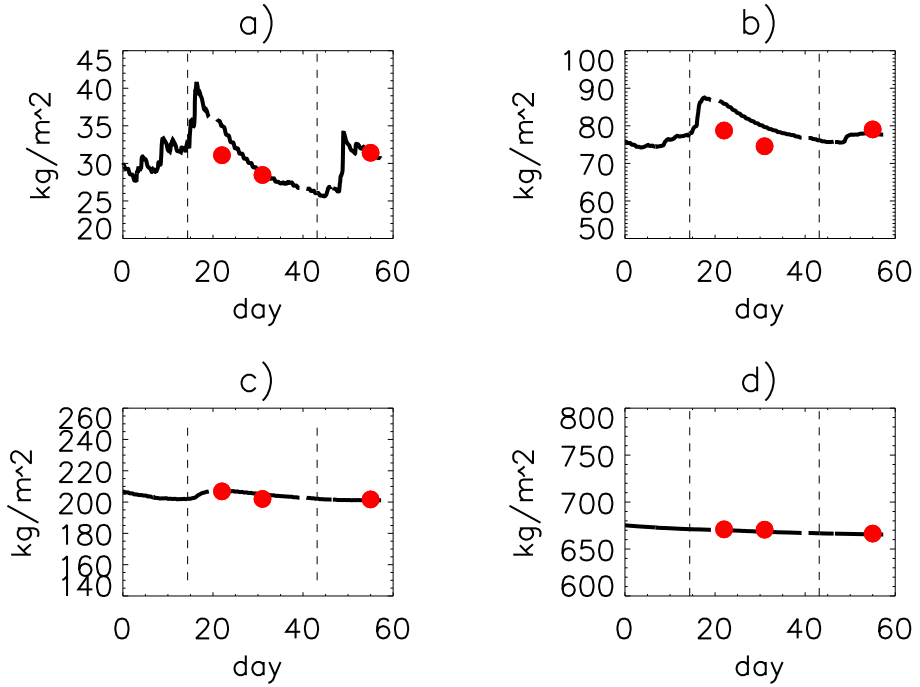

Figure 4. Evolution of the domain mean layer soil moisture content at different levels. Day number corresponds to the day since the start of the climatology simulation. Shaded circles show the values from corresponding IOP simulations. **(a–d)** correspond to increasing soil depths of 0.05, 0.225, 0.675 and 2.0 m. Vertical dashed lines mark 1 September and 1 October.

GMDD
8, 4453–4486, 2015

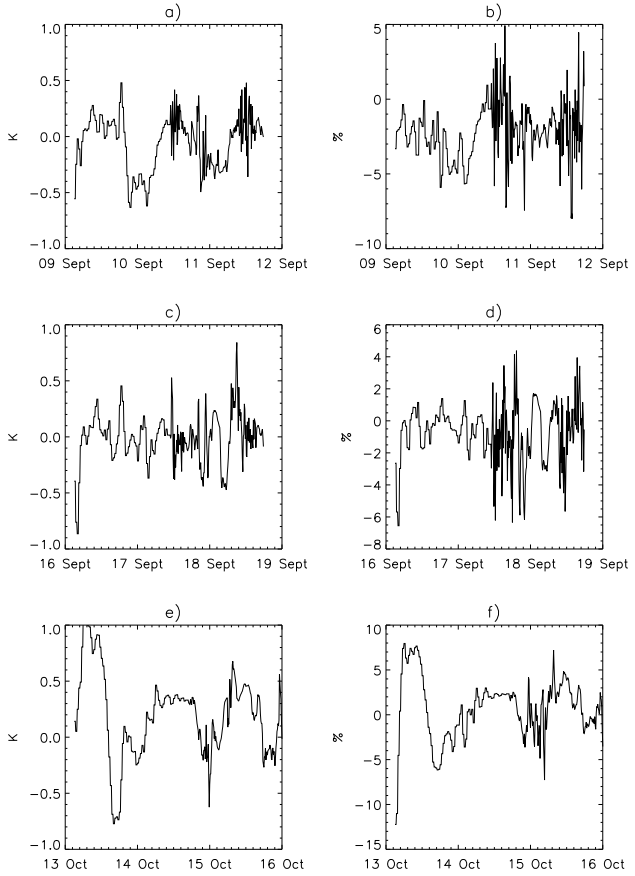

Figure 5. Difference between shorter IOP simulations and the longer climatology simulation (IOP minus climatology) for screen temperature **(a, c, e)** and relative percentage differences in screen-level specific humidity **(b, d, f)** at Duffryn for IOPs 4–5 **(a, b)**, IOPs 6–7 **(c, d)**, IOPs 8–9 **(e, f)**.

GMDD
8, 4453–4486, 2015

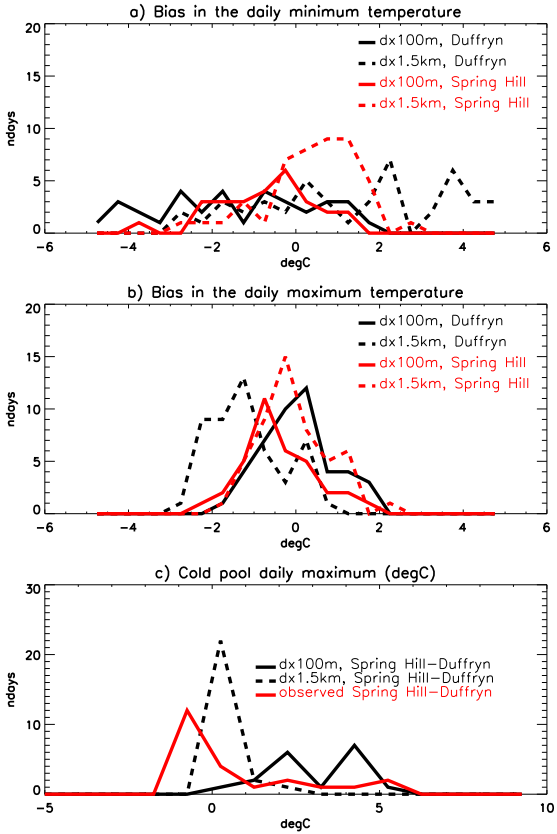

Figure 6. Bias in the model screen-level (1.5 m) temperatures (model minus observed). **(a)** Frequency distributions of daily hourly minimum temperature bias compared to observations at Spring Hill and Duffryn, **(b)** frequency distributions of daily hourly maximum temperature bias, **(c)** frequency distributions of cold pool strength, defined as the maximum daily difference between Spring Hill and Duffryn. The data are binned into intervals of width 0.5 K.

GMDD
8, 4453–4486, 2015

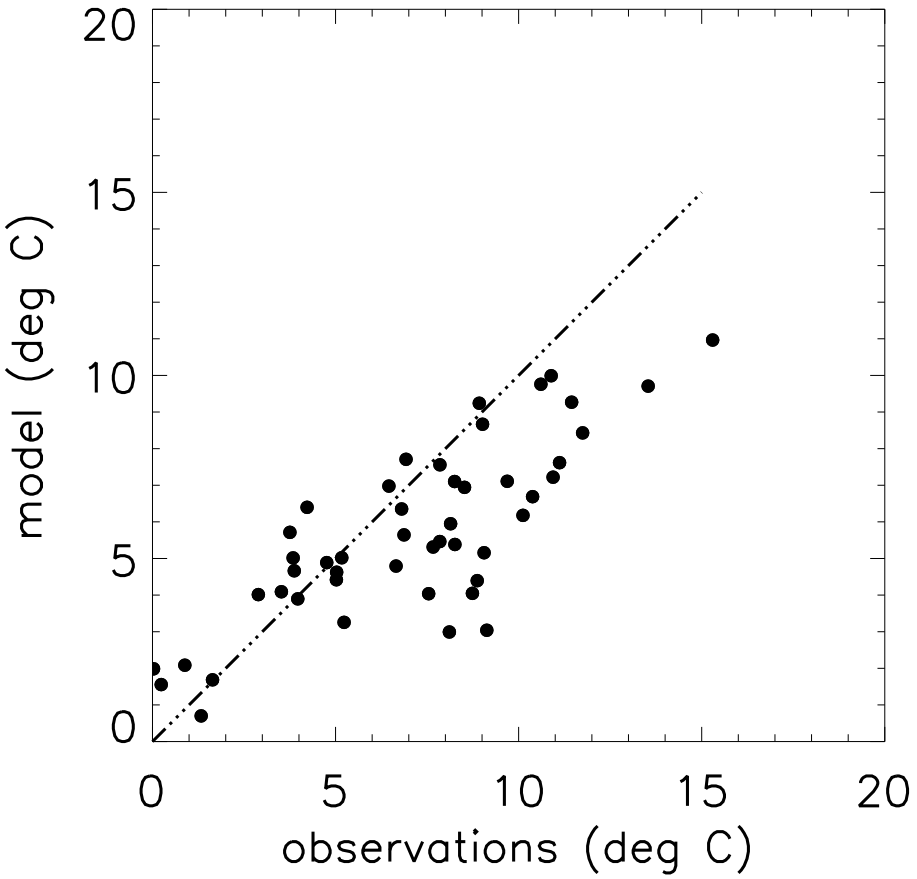

Figure 7. Simulated daily minimum Δ100 m screen temperatures vs. observations at Duffryn.

GMDD
8, 4453–4486, 2015

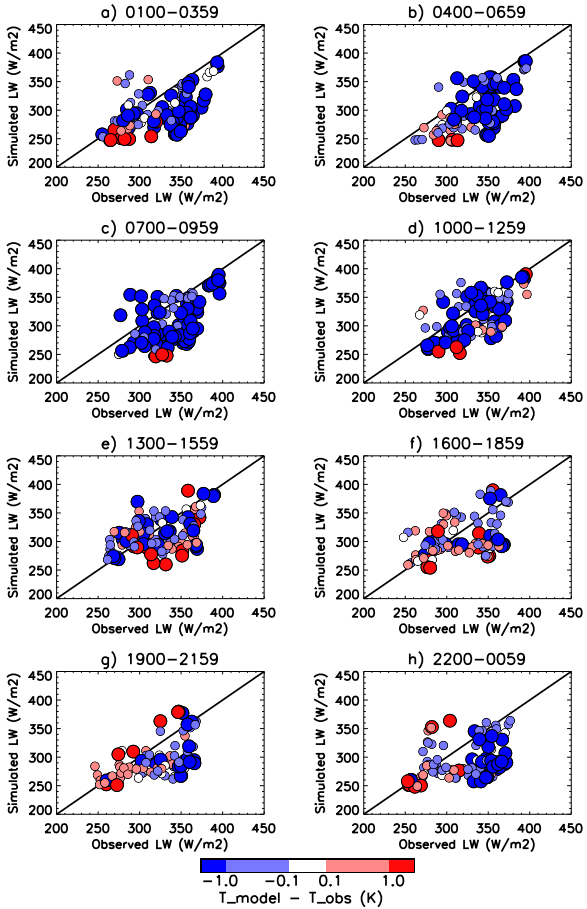

Figure 8. Bias in Δ100 m simulated downward longwave radiation and its relationship to bias in the screen level temperature, at Spring Hill. The temperature bias is represented as the colour and size of the marker (simulated – observed). Each marker represents mean hourly values.

GMDD
8, 4453–4486, 2015

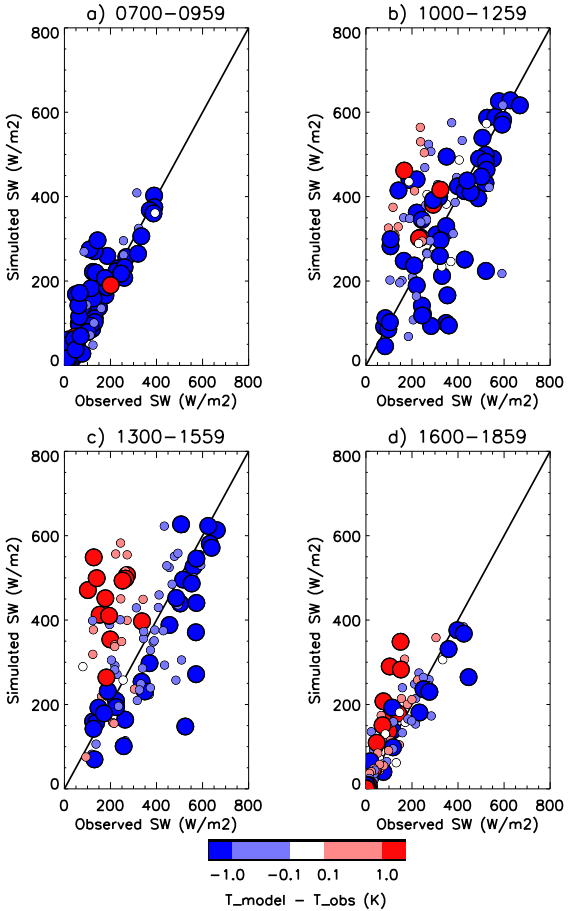

Figure 9. Bias in Δ100 m simulated downward shortwave radiation and its relationship to bias in the screen level temperature, at Spring Hill. The temperature bias is represented as the colour and size of the marker (simulated – observed).

GMDD
8, 4453–4486, 2015

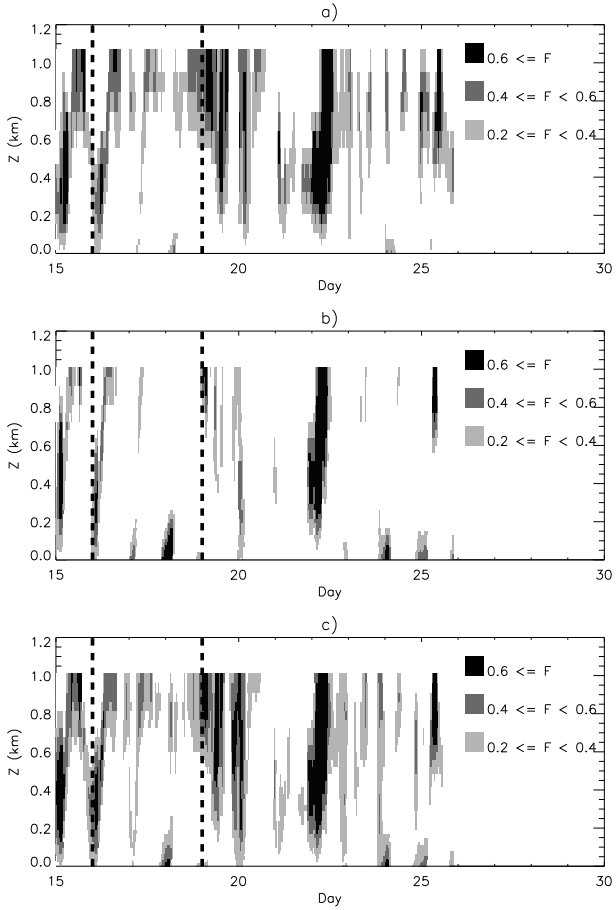

Figure 10. Hourly area averaged profiles of model cloud fraction for **(a)** Δ1.5 km, **(b)** Δ100 m and **(c)** Δ100 m_r. Vertical lines show 00:00 UTC 16 September and 00:00 UTC 19 September, and correspond to the period shown in Fig. 13.

GMDD
8, 4453–4486, 2015

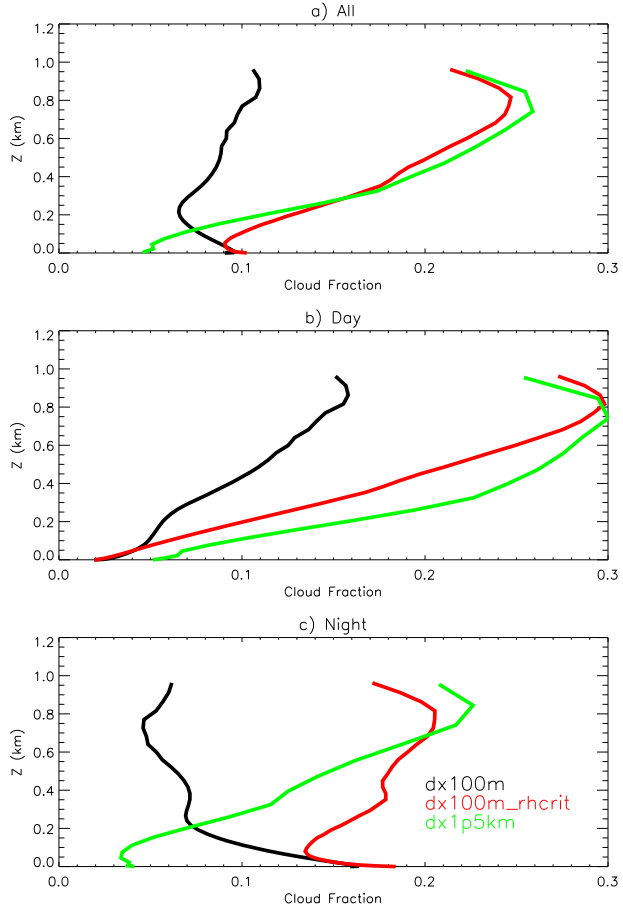

Figure 11. The mean cloud cover profile for the lowest kilometre for **(a)** all hours, **(b)** 07:00–19:00 UTC and **(c)** 19:00–07:00 UTC, averaged over all days in the re-run period (15–25 September).

GMDD
8, 4453–4486, 2015

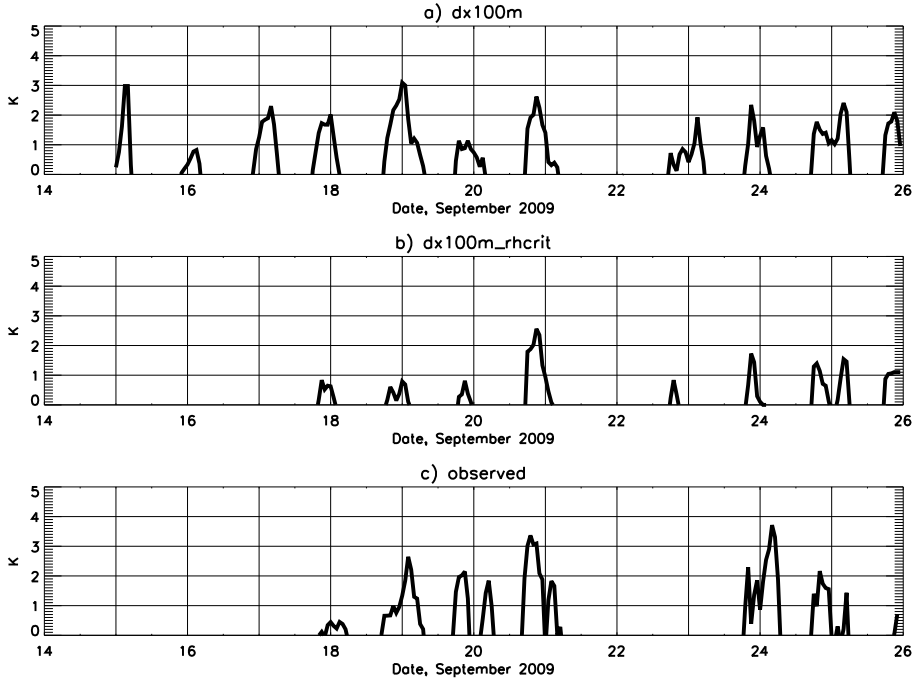

Figure 12. Impact of RH_{crit} profile change on the simulated cold pool strength, defined as the difference between screen temperature between Spring Hill and Duffryn (Spring Hill minus Duffryn). Positive values indicate the presence of cold air pools. **(a)** Δ100 m cold pool strength, **(b)** Δ100 m_r cold pool strength, **(c)** observed cold pool strength.

GMDD
8, 4453–4486, 2015

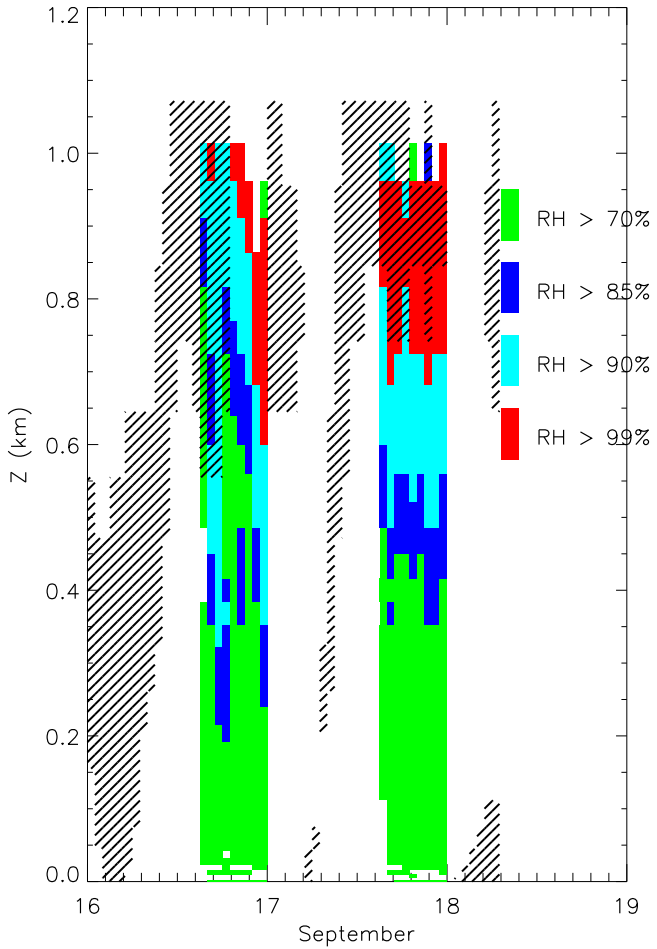

Figure 13. Radiosonde relative humidity profiles at Spring Hill during 16–18 September. Also shown are Δ1.5 km cloud fractions above 20 % (diagonal hatching).

GMDD
8, 4453–4486, 2015

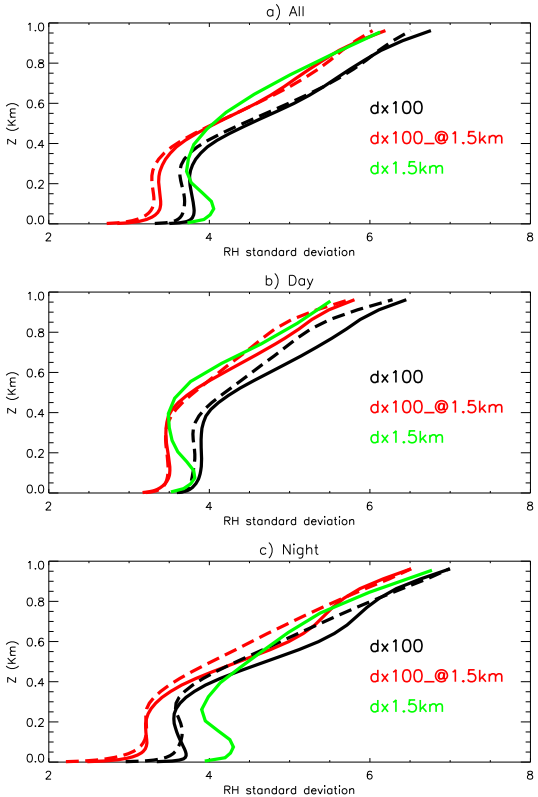

Figure 14. Standard deviations of relative humidity values simulated in, Δ100 m output (black), Δ100 m output averaged to 1.5 km resolution (red) and Δ1.5 km output (green). Solid lines are simulations with RH_{crit} profiles from the operational 1.5 km model, while dashed lines correspond to the RH_{crit} profile with higher thresholds described in Vosper et al. (2013a). The subfigures show **(a)** total mean profiles, **(b)** average day profiles (07:00–19:00 UTC) and **(c)** night profiles (19:00–07:00 UTC).

GMDD
8, 4453–4486, 2015